Theory and Experimental Realization of Negative Refraction in a Metallic Helix Array

Chao Wu,[1,2] Hongqiang Li,[1,2,*] Zeyong Wei,[1,2] Xiaotong Yu,[1,2] and C. T. Chan[3]

[1]*Physics Department, Tongji University, Shanghai 200092, China*

[2]*Shanghai Key Laboratory of Special Artificial Microstructure Materials and Technology, Shanghai, China*

[3]*Department of Physics, Hong Kong University of Science and Technology, Clear Water Bay, Kowloon, Hong Kong, China*

(Received 25 May 2010; revised manuscript received 6 November 2010; published 9 December 2010)

We developed a theory to compute and interpret the photonic band structure of a periodic array of metallic helices. Interesting features of the band structure include longitudinal and circularly polarized eigenmodes and wide polarization gap. The helical symmetry also implies unusual features such as negative group velocity bands at both sides of the polarization gap and band crossings pinned at the zone boundary. A direct proof of negative refraction via a chiral route is achieved for the first time by measuring the spatial beam shift through a slab of the three-dimensional helices.

DOI: 10.1103/PhysRevLett.105.247401 PACS numbers: 78.67.Pt, 42.25.Ja, 42.70.Qs

The prediction of negative refraction in chiral media [1] has fueled interest in chiral metamaterials as a medium to achieve a negative refractive index [2–5], strong optical activity [6–8] and circular dichroism [9–12]. In many recent studies, chiral metamaterials are typically realized as one or two layers of discrete chiral resonators, and the exotic properties are interpreted by a numerical approach assuming the applicability of effective medium theory [13]. A ''first-principles'' investigation starting from the real structure of the chiral building blocks would be fruitful for a deeper understanding of the relation between structure and functionality. As previous evidence of negative refractive behavior of chiral metamaterials was deduced by retrieving the constitutive parameters from the transmission and reflection spectra under normal incidence [2–5], a direct demonstration of negative refraction from chiral structures would be highly desirable.

Helix, as a representative element of helical symmetry, is intrinsically chiral because any object with helical symmetry does not have mirror symmetry. The rotation of the plane of polarization of electromagnetic (EM) waves by a twisted structure was observed as early as 1898 [14] and the observation of EM activity from randomly dispersed metallic helices in 1914 [14] ignited the interest in electromagnetic chirality. A helix has a continuous symmetry such that the system remains invariant if the helix is rotated in a given angular speed and simultaneously displaced at a corresponding speed along the helical axis. This special rotational or translational symmetry operation imposes an associated phase factor for the EM wave propagation [15,16]. As a consequence, the guided eigenmodes of metallic helix can have backward phase velocity [15,16]. It is expected that the structures comprising of helix units will provide us more options in wave manipulations by properly utilizing the electromagnetic chirality. By incorporating the constitutive relation of bianisotropic medium, an interesting paper presented an analytical model for helicoidal spirals [17], predicting the elliptical polarization of eigenstates and bandgaps along the directions orthogonal to the spiral axis. In an elegant recent experiment, very wide and robust polarization gaps were demonstrated in a gold helix metamaterial in the THz regime [18]. However, the underlying physics of such kind of chiral metamaterials are still under exploration.

In this Letter, we theoretically and experimentally investigate the properties of a three-dimensional structure made with a square array of metallic helices. Here, we will show that the special symmetry of a helix would guarantee the formation of longitudinal and circularly polarized eigenmodes, the existence of band crossing at the Brillouin zone (BZ) boundary and wide polarization gaps, as well as other important properties such as negative group velocity bands. We developed a photonic band theory for the helix array by combining multiple scattering theory [19,20] with Sensiper's solution for a single helix [15]. The theory enables us to identify interesting features such as the longitudinal and circularly polarized eigenmodes, the wide polarization gap, and negative group velocity bands at both sides of the gap. By measuring the spatial beam shift through a sample, we directly demonstrate the negative refraction in the helical systems for the first time.

Figure 1 shows a photograph of a sample of the square array of right-handed (RH) helices. Oriented along the

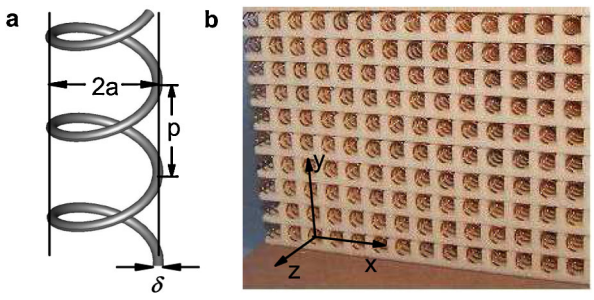

FIG. 1 (color online). (a) The schematic picture of a metallic helix unit and (b) photo of a square array of metallic helices.

z axis, the metallic helices form a square array in the xy plane with a lattice constant of $d = 11$ mm. Figure 1(a) shows the schematic picture of a single helix unit, which has a pitch of $p = 4.4$ mm, radius $a = 3.3$ mm, and diameter of metallic wires $\delta = 0.8$ mm. We define a pitch angle ψ by $\cot\psi = 2\pi a/p$. We note that a helix comes back to itself after being translated by a distance of Δz and being rotated simultaneously by an angle of $2\pi\Delta z/p$ (for RH helix) or $-2\pi\Delta z/p$ [for left-handed (LH) helix], and thus physical entities associated with the helix should satisfy the helical symmetry condition

$$U(\rho, \phi, z) = U\left(\rho, \phi \pm \frac{2\pi\Delta z}{p}, z + \Delta z\right) \tag{1}$$

with the $+(-)$ sign for the RH (LH) helix, respectively [15,16]. The periodicity along the helical axis also implies that the field components for an RH helix system can be expanded by functions of the form

$$\psi_n(\rho, \phi, z) = e^{ik_z z} F_n(\rho) e^{-in\phi} e^{i(2n\pi/p)z} \tag{2}$$

where k_z is the Bloch wave vector along z axis. The angular term should be $e^{in\phi}$ instead if the helix is LH. The radial function $F_n(\rho)$ obeys the Helmholtz differential equation, and can be expressed in terms of modified Bessel functions I_n and K_n. We follow the Sensiper approach [15] to impose the condition of uniformly distributed surface current flow along the metal wires. Under that assumption, the boundary continuity conditions require that the local electric field on metal wires must be perpendicular to the line of metal wire. Combining with the multiple scattering theory formalism which accounts for interhelix coupling, we derive an eigenvalue equation of helix array as

$$\sum_n \left[\left(k_z^2 a^2 - k^2 a^2 + \frac{n^2 k^2}{\tau_n^2}\cot^2\psi\right) y_n I_n(\tau_n a) + k^2 a^2 \cot^2\psi z_n I_n'(\tau_n a)\right] \frac{R_n}{x_n \tau_n} = 0 \tag{3}$$

where $\tau_n = [(k_z + \frac{2\pi n}{p})^2 - k^2]^{1/2}$, $R_n = \frac{\sin(n\pi\delta/p)}{n\pi\delta/p}$, $y_n = K_n(\tau_n a) + (-1)^n \sum_l S_{l-n}(\tau_n) I_l(\tau_n a)$, $z_n = K_n'(\tau_n a) + (-1)^n \sum_l S_{l-n}(\tau_n) I_l'(\tau_n a)$, $x_n = y_n I_n'(\tau_n a) - z_n I_n(\tau_n a)$, and $S_l(\tau) = \sum_{q\neq 0} K_l(\tau R_q) e^{il\phi_q} e^{i\mathbf{k}_i\cdot\mathbf{R}_q}$ is a lattice sum running over the nodes (R_q, ϕ_q) of the square lattice in cylindrical coordinates with $\boldsymbol{k}_\mathbf{i}$ being the transverse component of the wave vector $\boldsymbol{k}$ in the air, and $I_n'(x)$, $K_n'(x)$ satisfying to $I_n'(x) = dI_n(x)/dx$, $K_n'(x) = dK_n(x)/dx$.

The computed photonic band structures give us an intuitive understanding of the optical property of helix arrays. In the helical structure, there is a $\pm\pi/2$ phase difference between the radial and the angular components for both the electric field and magnetic field, implying that the eigenmodes are left-handed or right-handed circularly polarized (LCP or RCP). This can be checked by examining the field solutions written in the Sensiper form (see supplementary material, Ref. [21]) [15]. Figures 2(a)–2(c) show the band structure of the helix metamaterials along the helix axis for three lattice constants $d = 20$ mm, 11 mm, and 8 mm, respectively. We label the eigenmodes in Fig. 2 by their dominant term in Eq. (2). For example, the $(-1, S)$ modes (blue stars in Fig. 2) have $n = -1$ term as the dominant term and "S" stands for a "slow mode" below the light line, and we use the subscript "F" for a mode inside the light cone. The polarization of an eigenmode is analyzed in Fig. 3 by the ratios $|\langle E_z\rangle|/|\langle E_x\rangle|$, $|\langle E_z\rangle|/|\langle E_y\rangle|$, and $\mathrm{AR} = \langle E_x\rangle k_z/\langle iE_y\rangle|k_z|$, where the spatial average $\langle\cdots\rangle$ is taken inside a unit cell. Figures 3(a) and 3(b) clearly indicate that the (0) mode (red circles in Fig. 2), has a strong longitudinal component E_z and this mode picks up a circular polarized character as k_z increases. It goes to a longitudinal mode with a finite frequency at the BZ center ($k_z = 0$). Both the electric field and magnetic field are essentially parallel to the helical axis. It is evident from Fig. 2 that the interhelix coupling pushes the longitudinal mode to higher frequencies. In the limit $d \to \infty$, it goes to zero frequency. Figures 3(c)–3(f) show that the $n = \pm 1$ modes are either LCP or RCP. Eigenmode analysis and numerical transmission simulation employing a finite thickness slab showed that the $n = -1$ modes with positive group velocity couple to an incident plane wave with opposite handedness as the helix, while the $n = +1$ modes with positive group velocity (green squares in Fig. 2) couple to incident waves of the same handedness as the helix. In general, a mode couples to an incident wave of the same (opposite) handedness as the helix if $nk_z > 0 (< 0)$.

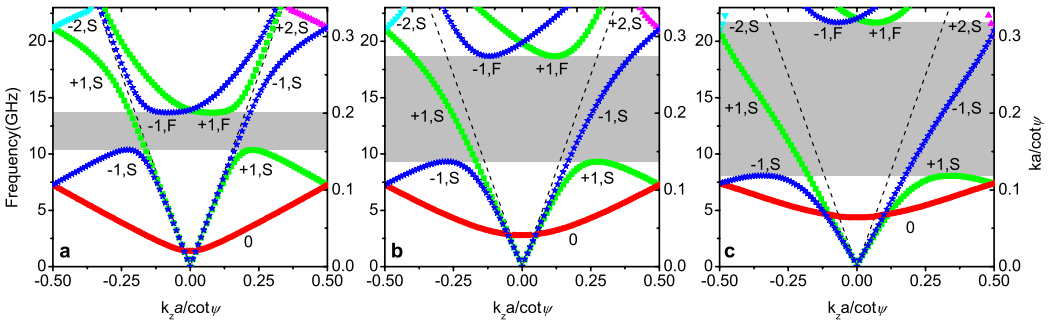

FIG. 2 (color online). The photonic band structures of the helix crystal along the helix axis for three lattice constants (a) $d = 20$ mm, (b) $d = 11$ mm, (c) $d = 8$ mm. The pitch $p = 4.4$ mm, the radius $a = 3.3$ mm, and diameter of metallic wires $\delta = 0.8$ mm.

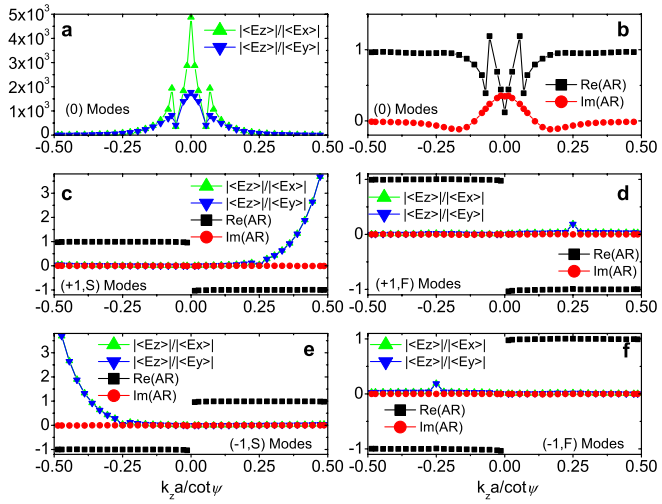

FIG. 3 (color online). Eigenmode analysis by calculating the ratios $\mathrm{AR} = \langle E_x\rangle k_z/\langle iE_y\rangle|k_z|$ (black squares for real, red circles for imaginary), $|\langle E_z\rangle|/|\langle E_x\rangle|$ (green up-triangles) and $|\langle E_z\rangle|/|\langle E_y\rangle|$ (blue down-triangles). (a) and (b) for $n = 0$ modes; (c) $(+1, S)$ modes; (d) $(+1, F)$ modes; (e) $(-1, S)$ modes; (f) $(-1, F)$ modes.

An important feature of the band structure is the existence of a wide polarization gap (shaded in grey in Fig. 2) that only allows incident waves of opposite handedness to pass through. As such, a RH helix array has an RCP gap. The gap grows wider for a higher helix filling ratio (smaller d). Such wide polarization gaps have been experimentally demonstrated for a thin slab of gold helices in IR frequencies [18,22]. The lower edge of the polarization gap is pinned at the frequency at which the $(+1, S)$ mode attains zero group velocity. The $(+1, S)$ mode is the result of the hybridization between the free photons (riding on the light line) and a mode guided on the helix which is backscattered by the periodicity. As the $(+1, S)$ mode is guided on the helices, the frequency is only moderately affected by the interhelix coupling. The upper edge of the polarization gap is pinned at the frequency at which the $(+1, F)$ mode has zero group velocity. The $(+1, F)$ mode is the result of hybridization between the radiative modes from helix and free photons. It exists as an eigenmode in the periodic array and is sensitive to the volume available between the helices. The mode is squeezed to higher frequencies at a higher helix filling ratio, leading to a much wider polarization gap for smaller values of the lattice constant (d). In order words, the lower edge of the gap is primarily determined by the helix parameters (a and p) along the helical axis, while the upper edge is primarily determined by the structural parameter perpendicular to the helical axis (lattice constant d). This picture explains why the polarized gap can be very wide in the frequency range.

Another interesting feature of the band structure is the emergence of the negative group velocity bands at both sides of the polarization gap, which is different from the previous theoretical prediction that the negative refraction only happens above the resonant gap [1]. Both the high frequency $(+1, F)$ and the lower frequency $(+1, S)$ branch exhibit negative group velocities. The $(+1, S)$ branch exhibits negative group velocity after reaching a maximum frequency that pins the lower edge of the polarization gap. Concomitant with the negative refraction bands in the slow mode, one can see from Fig. 2 that there are band crossings at the BZ boundary ($k = \pi/p$) and the degenerate modes are pinned at frequencies (see supplementary material, Ref. [21]) that are nearly independent of the lattice constant d. We note that according to Eq. (2) Bloch modes that differ by $\Delta k = 2\pi/p$ will be orthogonal because of orthogonality of the angular phase factor. Consequently, the (0) branch is degenerate with the $(+1, S)$ branch at the zone boundary, which ensures the existence of a negative group velocity branch below the polarization gap. This is essentially a consequence of backward waves guided on a metallic helix satisfying the helical symmetry. A comparative study shows that the genuine longitudinal and/or circularly polarized eigenmodes, the negative dispersion bands in the slow mode, and band crossing will disappear when the helices are cut into "discrete" spirals (see supplementary material, Ref. [21]). The slope of the negative dispersion band above the polarization gap becomes very small without the helical symmetry. Thus we conclude that many salient features of the band structure are direct consequences of the helical symmetry requirement [Eq. (1)].

We performed negative refraction measurements inside an anechoic chamber through a slab of the helix array with the aforementioned geometric parameters [the band structure is shown in Fig. 2(b)]. Helix samples are fabricated by periodically embedding the clockwise metallic helices in a polyurethane foam slab. The polyurethane foam is lossless with $\varepsilon \approx 1$. The sample slab contains 15×11 metallic helices, each having 140 periods along the helical axis (z axis).

Computed equifrequency surfaces (EFSs) for the $(+1, S)$ branch [see Fig. 4(b)] and $(+1, F)$ branch (not shown) demonstrate that negative refraction can be achieved at both sides of the polarization gap. Here we try to realize the negative refraction at the lower edge of the gap, which is not found or predicted in other systems before. As the $(\pm 1, S)$ modes lie below the light line, we can excite the $(\pm 1, S)$ modes by prism coupling techniques to penetrate a Gaussian beam into the sample slab [see Fig. 4(a)], and estimate the refractive angle quantitatively by measuring the spatial beam shift. Figure 4(a) illustrates the schematic configuration of our experimental setup. Two isosceles right-angled triangular alumina prisms ($\varepsilon_r = 8.9$) are placed so that they touch the sample slab at both sides and a Gaussian beam is normally incident in xz plane to the air-prism interface from a linearly polarized horn emitter, ensuring an incident angle of 45° from alumina to sample. The local field intensity is measured by the LCP/RCP horn receiver as a function of the horizontal position in a precision of 1 mm per step. The spatial shift of the outgoing beam is found by measuring the peak position at

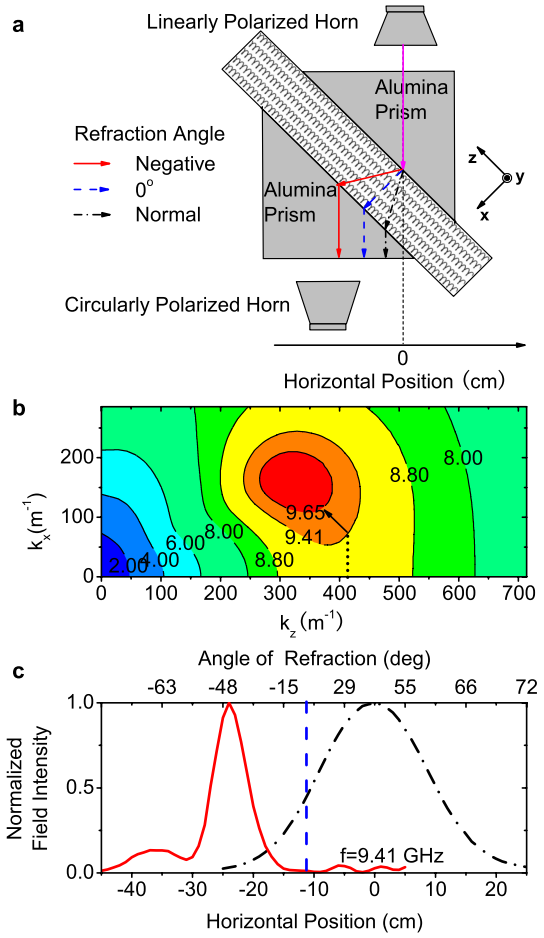

FIG. 4 (color online). (a) Schematic of the experimental setup for negative refraction. (b) Computed equifrequency surface (EFS) for the (+ 1, S) branch. The arrow refers to the direction of the refracted waves at 9.41 GHz under an incident angle at 45°. (c) Measured electric field intensity as a function of the horizontal position of the circularly polarized horn receiver, with (red) or without (black) the chiral sample and alumina prisms at 9.41 GHz. The two curves are normalized such that the magnitude of both peaks is unity. The blue dashed line at the horizontal position of −11 cm refers to the spatial beam shift with respect to 0° refracted angle.

the interface of prism. The coordinate origin in the horizontal position is aligned with the position of the horn emitter, marked by the dashed vertical line in Fig. 4(a). Negative refraction is observed from 9.18 GHz to 9.48 GHz with a refraction angle from −17.44° to −50.11°, which is in good agreement with the computed EFS shown in Fig. 4(b). The solid line in Fig. 4(c) presents the spatial profile of local field intensity measured at 9.41 GHz. A peak value is measured at the horizontal position of −24 cm, corresponding to a refraction angle of −46.5°, roughly equal to −45.8° estimated by EFS analysis. Thus negative refraction below the polarization gap is verified experimentally. We note from Fig. 4(b) that in the frequency range of our interest, the dispersion is not only negative along k_z, but it is also negative along k_x due to Bragg scattering.

In summary, the unusual optical properties in metallic helix arrays are revealed by the photonic band structure computed by a semianalytical technique. There are negative bands both above and below the polarization gap. Negative refraction on the low frequency branch is demonstrated directly by measuring the spatial beam shift. We note that the optics of the helix array is governed by the helical symmetry as well as scatterings within the helix lattice and there is no easy way to describe the phenomenon using effective medium parameters.

This work was supported by NSFC (No. 10974144, 60674778), HK RGC Grant No. 600308, the National 863 Program of China (No. 2006AA03Z407), NCET (07-0621), STCSM and SHEDF (No. 06SG24). We thank Professor M. Wegener and Dr. J. Gansel for helpful discussions.

*hqlee@tongji.edu.cn

[1] J. B. Pendry, Science **306**, 1353 (2004).
[2] E. Plum *et al.*, Phys. Rev. B **79**, 035407 (2009).
[3] S. Zhang *et al.*, Phys. Rev. Lett. **102**, 023901 (2009).
[4] J. Zhou *et al.*, Phys. Rev. B **79**, 121104 (2009).
[5] M. C. K. Wiltshire, J. B. Pendry, and J. V. Hajnal, J. Phys. Condens. Matter **21**, 292201 (2009).
[6] E. Plum *et al.*, Appl. Phys. Lett. **90**, 223113 (2007).
[7] H. Liu *et al.*, Phys. Rev. B **76**, 073101 (2007).
[8] T. Q. Li *et al.*, Appl. Phys. Lett. **92**, 131111 (2008).
[9] S. L. Prosvirnin, and N. I. Zheludev, Phys. Rev. E **71**, 037603 (2005).
[10] A. V. Krasavin *et al.*, Appl. Phys. Lett. **86**, 201105 (2005).
[11] V. A. Fedotov *et al.*, Phys. Rev. Lett. **97**, 167401 (2006).
[12] E. Plum *et al.*, Phys. Rev. Lett. **102**, 113902 (2009).
[13] N. Engheta, D. L. Jaggard, and M. W. Kowarz, IEEE Trans. Antennas Propag. **40**, 367 (1992); S. Tretyakov *et al.*, J. Electromagn. Waves Appl. **17**, 695 (2003); T. G. Mackay and A. Lakhtakia, Phys. Rev. E **69**, 026602 (2004); C. Monzon and D. W. Forester, Phys. Rev. Lett. **95**, 123904 (2005); Q. Cheng and T. J. Cui, Phys. Rev. B **73**, 113104 (2006).
[14] J. C. Bose, Proc. R. Soc. London **63**, 146 (1898); I. V. Lindell, A. H. Shivola, S. A. Tretyakov, and A. J. Viitanen, *Electromagnetic Waves in Chiral and BI-Isotropic Media* (Artech House, Norwood, MA, 1994).
[15] S. Sensiper, Proc. IRE **43**, 149 (1955).
[16] J. R. Pierce, Proc. IRE **35**, 111 (1947).
[17] P. A. Belov, C. R. Simovski, and S. A. Tretyakov, Phys. Rev. E **67**, 056622 (2003).
[18] J. K. Gansel *et al.*, Science **325**, 1513 (2009).
[19] S. K. Chin, N. A. Nicorovici, and R. C. McPhedran, Phys. Rev. E **49**, 4590 (1994).
[20] N. A. Nicorovici, R. C. McPhedran, and L. C. Botten, Phys. Rev. E **52**, 1135 (1995).
[21] See supplementary material at http://link.aps.org/supplemental/10.1103/PhysRevLett.105.247401.
[22] J. K. Gansel *et al.*, Opt. Express **18**, 1059 (2010).